J Mater Sci: Mater Electron (2015) 26:8652–8662
DOI 10.1007/s10854-015-3540-z

Investigation on magnetic and electric properties of morphologically different perovskite $LaFeO_3$ nanostructures

S. Thirumalairajan[1,2] · K. Girija[2] · Valmor R. Mastelaro[1] · N. Ponpandian[2]

Received: 10 May 2015 / Accepted: 24 July 2015 / Published online: 29 July 2015
© Springer Science+Business Media New York 2015

Abstract In the present study, investigation on magnetic and electric properties of $LaFeO_3$ nanostructures like nanopetals, dendrites, nanorods and nanospheres prepared by surfactant-assistant hydrothermal process were performed. X-ray powder diffraction pattern of all the prepared samples exposed the formation of the single phase orthorhombic crystals. Transmission electron microscopy images revealed the shape and size of the synthesized $LaFeO_3$ nanostructures and were found to be in the range ~50–90 nm. The weak ferromagnetic behaviour of the as prepared nanostructures was exhibited using vibrating sample magnetometer at room temperature. The activation energy for electrical conduction has been calculated from the Arrhenius plot using impedance measurement. The activation energy for the grain conduction was found to be in the range 0.110–0.142 eV for different $LaFeO_3$ nanostructures. Temperature and frequency dependent dielectric properties were investigated and found to be two orders of magnitude higher than the other reported perovskite oxide materials. The excellent combination of magnetic and electric properties of $LaFeO_3$ nanostructure materials is found to be suitable for use in high-frequency applications.

✉ S. Thirumalairajan
sthirumalairajan@gmail.com

[1] Instituto de Física de São Carlos (IFSC), University de São Paulo, CP 369, São Carlos, SP 13560-970, Brazil

[2] Department of Nanoscience and Technology, Bharathiar University, Coimbatore 641 046, India

1 Introduction

The nanocrystalline materials have received extensive attention due to their unique physical and chemical properties. The properties of these materials are entirely different from their conventional polycrystalline counterparts due to their unique structure. Also, the shape and structure property relationship of nanocrystalline materials differ considerably from those observed for the bulk materials [1–3]. The changes in the properties of nanomaterials are mainly attributed to the increase in the fraction of atoms on the surface as compared to the bulk and also the dominance of the quantum effect associated with the reduction of the crystallite size. The alterations in the physical properties enhances their applicability in solid oxide fuel cells, ultrasensitive magnetic read heads, sensors and magnetic memory cells [4–6]. The ability to tune the size, morphology, magnetic and electrical properties to remarkable progress has been recently made possible by the aqueous synthesis of perovskite oxide nanomaterials [7, 8].

Perovskite oxides have been of great importance since the material exhibits a wide range of unusual properties which include magnetic, superconducting and dielectric [9, 10]. Perovskites come under the formula ABO_3, where A is an alkali rare earth like La, Ca, Sr, Ba, etc., and B is an element with valence +3 or +2, such as Fe, Cu and Ni which exhibits high proton and oxygen ion conductivity [11–13]. It is expected that mixed ionic and electronic conductors may be present in these compounds if the B-site is partially substituted by the appropriate first row transition elements. It has been reported that Fe-containing perovskite exhibits high O^{2-} ion and electronic conductivity [14–16]. Synthesis of perovskite oxide with stable structure and unique shape is a challenging topic of research in the area of materials science. Particularly,

magnetic (Fe and Ni) perovskite nanomaterials continue to be interesting from both the scientific and technology point of view [17–20]. The impedance analysis has been widely used to study the dielectric behaviour of the crystalline and polycrystalline ceramic materials. In addition, the dielectric properties of ferroelectromagnetic materials arise due to intra-grain, inter-grain and the electrode effects. The motion of charges could take place by charge displacement, dipole reorientation and space charge formation etc., [21–23]. In order to understand the electrical properties of a given sample, the grain and grain boundary contributions must be separated out. Impedance analysis has emerged as a powerful tool for separating out these contributions.

Recently, our group has been involved in the synthesis of different $LaFeO_3$ nanostructures which includes the nanocubes, nanorods, nanospheres, microspheres and dendrites using facile and environment friendly wet chemical methods by precisely controlling the nature of precursor and experimental conditions. In the previous work reported by us elsewhere, we have elaborated the effect of the precursors and preparatory methods in the formation and growth of the different $LaFeO_3$ nanostructures [24–27]. However, to our knowledge reports which explore the dependence of physical properties on the shape of $LaFeO_3$ nanostructures are not available. The present work deals with the systematic investigation of magnetic and electric properties of well defined $LaFeO_3$ morphologies like nanopetals, dendrites, nanorods and nanospheres with crystallite size below 100 nm.

2 Characterization measurements

The structure, size and shape of the prepared samples were characterized using X-ray diffraction [(XRD), Bruker Germany D8 Advance] with $CuK_{\alpha 1}$ radiation ($\lambda = 1.54$ Å) and transmission electron microscopy (TEM, JEM 2100 F) with an acceleration voltage of 200 kV by placing the powder on a copper grid. The magnetic properties were analysed using vibrating sample magnetometer (VSM) (EG & G, PARC) with an applied magnetic field of 20 kOe at room temperature. The impedance measurements were performed for all the samples. The samples of $LaFeO_3$ nanostructures were sieved and cold isostatically pressed at 300 MPa into cylindrical pellets of 8 mm diameter and ~2 mm thickness for the impedance measurement. AC impedance spectroscopic measurements have been carried out using a Hewlett–Packard HP 4284A model Precision LCR Meter over the frequency range from 1 to 20 Hz in the temperature domain 300–340 K. The electrical conductivity value was estimated using the relation $\sigma = t/(R_bA)$, where t is the thickness of the specimen, A the area covered by the silver electrodes in contact with the specimen and R_b is the bulk resistance of the material derived from the intercept of the complex impedance plot i.e., Nyquist plot on the real axis.

3 Results and discussion

3.1 Structural analysis

$LaFeO_3$ samples with different morphologies were prepared by the surfactant assisted hydrothermal process using different precursor and surfactant as described in detail in our previous report [24–27]. The phase, purity and crystallinity of different $LaFeO_3$ nanostructure samples prepared with soft surfactant were determined using powder XRD measurements. Figure 1 represents the XRD pattern of the $LaFeO_3$ nanopetals, dendrites, nanorods and nanospheres calcinated at 800 °C for 2 h respectively. The peaks observed in the XRD pattern indicate that all the samples crystallize as a perovskite phase with orthorhombic structure. The lattice parameters estimated from XRD pattern was found to be $a = 5.565$, 5.569, 5.572 and 5.575 Å, $b = 7.838$, 7.843, 7.845 and 7.849 Å and $c = 5.577$, 5.581, 5.584 and 5.587 Å for the $LaFeO_3$ nanopetals, dendrites, nanorods and nanospheres, with a maximum experimental error of ±0.0003, which is in good agreement with the results reported in literature (JCPDS 37-1493) [28]. The narrow sharp peaks and the absence of impurity peaks suggest that the $LaFeO_3$ products are highly pure and crystalline. The bulk density of compressed $LaFeO_3$ powder is 6.555 g cm^{-3} [29]. The density of $LaFeO_3$ nanostructures for all the samples was estimated from the XRD data and found to be in the range 6.72–6.95 g cm^{-3}.

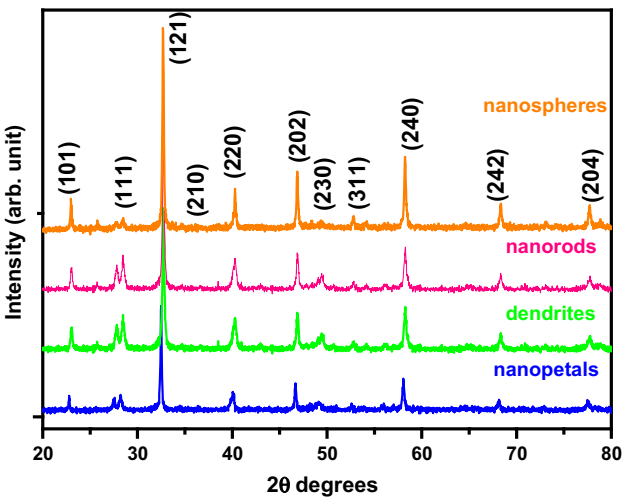

Fig. 1 X-ray diffraction pattern of different $LaFeO_3$ nanostructures

The $\beta\cos\theta$ value calculated from the Williamson–Hall plot for the prominent peak (121) was used in the Scherrer's formula [29] to calculate the average crystallite size and was found to be ~92, 81, 63 and 51 nm for the prepared nanopetals, dendrites, nanorods, and nanospheres respectively. These values are found to be in agreement with the results obtained from the morphological analysis section.

3.2 Morphology analysis

The shape and size of the prepared different $LaFeO_3$ nanostructures was examined using TEM analysis. In Fig. 2a, the nanoparticles forming the nanopetals with an average size of ~90 nm obtained using the PVP surfactant can be observed. Figure 2b reveals the clear, well defined and uniformly ordered dendrite structures with distinct trunk and branches distributed on both sides of the trunk when cationic surfactant CTAB was used. The overall length of the dendrite branches range between 1 and 1.5 μm, with diameter ~85 nm. $LaFeO_3$ nanorod structures observed in Fig. 2c was obtained when urea was employed as the structure directing agent. A close observation reveals that the diameter of single nanorod is ~0 nm and length ~240 nm with aspect ratio ~4. When citric acid was used as the structure directing agent, nanospheres as shown in Fig. 2d with average particle size 50 nm were obtained. The surface area of the prepared nanostructures were measured using Brunauer–Emmett–Teller analysis and were found to be 42.4, 48.8. 68.5 and 90.25 m^2g^{-1} for nanopetals, dendrites, nanorods and nanospheres. As the particle size decreases the surface area increases and also due to the effect of interparticle spacing.

Thus by correlating the outcome from TEM images it can be concluded that the observed results are in good agreement with the XRD pattern. We have reported a detailed analysis on the preparation of nanopetals, dendrites, nanorods and nanospheres along with the effect of the nature of precursor, different growth conditions, plausible growth mechanism and their potential applications in our previous publications [24–27]. The above obtained different $LaFeO_3$ nanostructures were used for further analysis to understand their shape and size effect on the magnetic and electric properties in the present study.

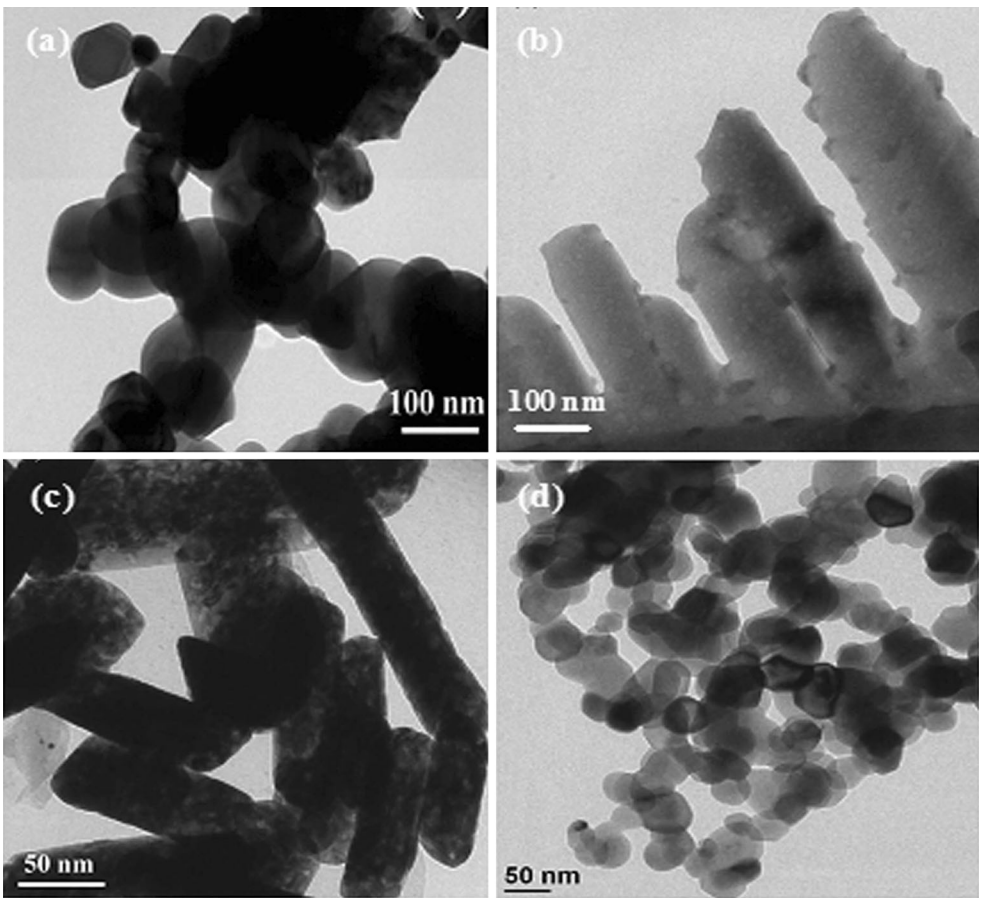

Fig. 2 TEM images of different $LaFeO_3$ nanostructures **a** nanopetals, **b** dendrites, **c** nanorods and **d** nanospheres

3.3 Morphology based magnetic properties of $LaFeO_3$ nanostructures

The magnetic behaviour of $LaFeO_3$ nanostructures with different morphologies and also particle size have been studied by measuring and analysing the magnetic hysteresis using VSM at room temperature under maximum applied magnetic field of 20 KOe. The M-H loop of the four different $LaFeO_3$ morphologies is shown in Fig. 3a–d. The hysteresis loops almost attain saturation at the maximum applied magnetic field. This indicates the presence of large anisotropy and uncompensated surface spins, i.e., the presence of more surface atoms in the nanomaterials. The net magnetization of $LaFeO_3$ is very small because of the antiferromagnetic order of the Fe^{3+} spins. The slight canting of Fe^{3+} spins produces weak ferromagnetism. The spontaneous magnetization reported for bulk $LaFeO_3$ crystals are ~0.1 emu/g at room temperature [30]. All the morphologies exhibit the hysteresis features and the shape of the loops represent small spontaneous magnetization suggesting weak ferromagnetic behaviour at room temperature.

The nature of domain in a weak $LaFeO_3$ ferromagnetic material having particular shape and size can be determined by calculating the M_r/M_s value from the hysteresis loop and was found to be 0.1837, 0.2096, 0.2137 for nanopetals, dendrites and nanorods respectively, suggesting the presence of pseudo-single domains (PSD). The value of $LaFeO_3$ nanospheres was 0.0231 which suggest the formation of superparamagnetic (SPM) effect due to the small particle size and uniform shape. In addition, the distinction between single domain (SD) and multi domain

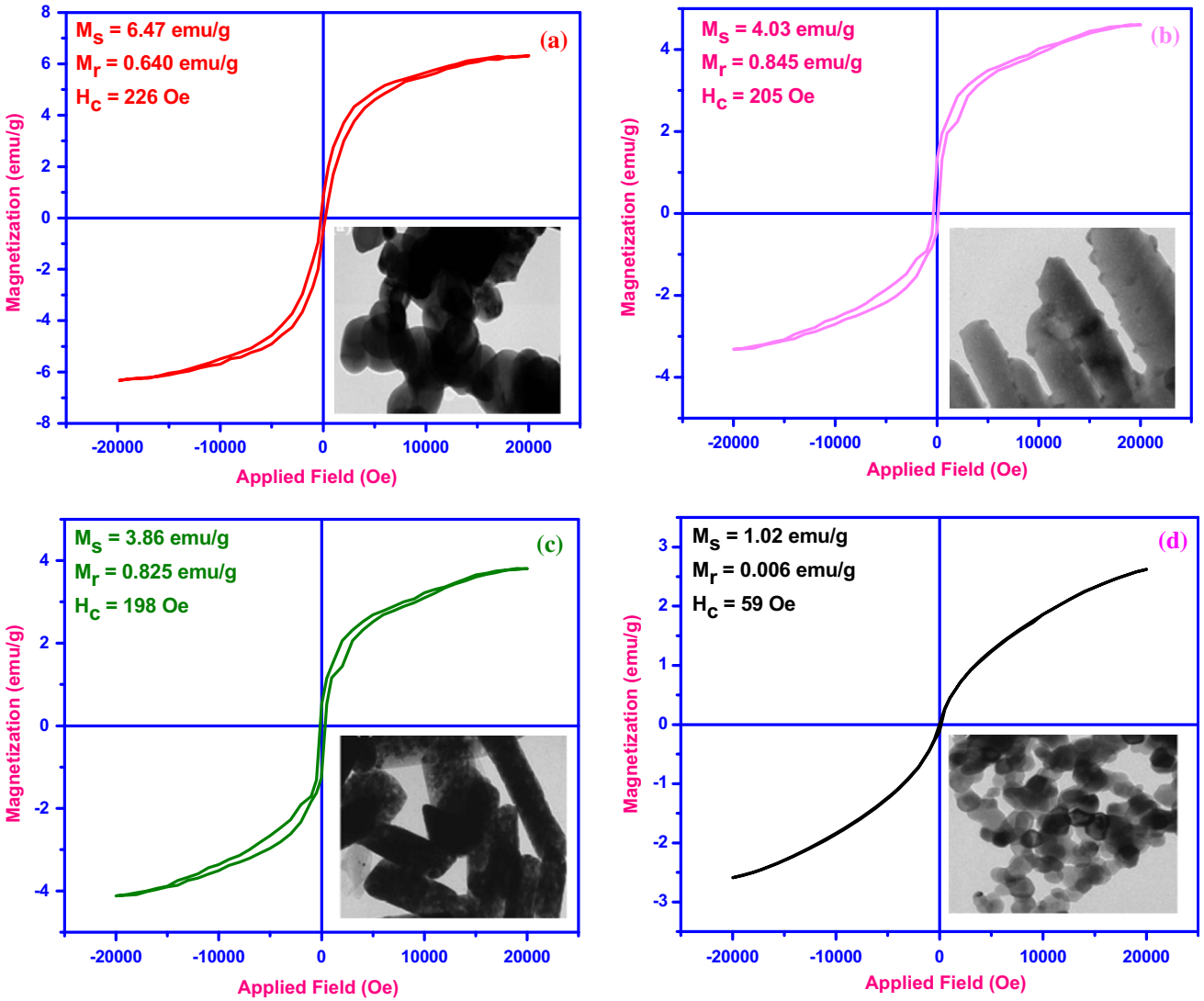

Fig. 3 Room temperature M–H loop of the different $LaFeO_3$ nanostructures and in the *inset* (*left*) is the values of M_s, M_r and H_c, (*right*) the corresponding TEM images of the nanostructures

(MD) is straightforward. However, small MD grains exhibit a mixture of SD like (high remanence) and MD like (low coercivity) behaviour. This state is called pseudo single domain (PSD), which occurs in smaller particles with few multi-domain grains. A particle size continues to decrease with the SD range; the critical threshold is reached at which remanence and coercivity goes to zero ($LaFeO_3$ nanospheres). When this happens, the grain becomes superparamagnetic (SPM).

The coercivity of particles has a striking dependence on their size and shape. It is typically found that the coercivity decreases, goes through a minimum and then tends towards zero. The maximum coercivity for a given material occurs within its PSD range, which is characterized by the presence of multi domains in smaller particles [30]. For larger grain size, coercivity decreases as the grain subdivides into domains. For grain size lesser than the PSD range, the particles are purely SD. For very small grain size, coercivity again decreases, because of the randomizing effect of thermal energy as in superparamagnetisim. The PSD range thus marks an upper limit to the SD range and lower limit to the MD range. The presence of PSD and SPM reflects in the coercivity value, which is highly sensitive to the variation in size, shape, aspect ratio and synthesis condition of the sample. These values determine the use of the magnetic materials for specific magnetic applications. The present study concentrates the dependence of size and shape on the properties of $LaFeO_3$ nanostructures. An initiative was taken to understand the reason underlying the variation of coercivity among the different morphologies of $LaFeO_3$. The prepared $LaFeO_3$ nanostructures are weak ferromagnetic and multi disperse system consisting of the SD and MD particles. The magnetization of the sample is considered as the sum of two terms:

$$M(H) = M^f H + M^{sp}(H) \tag{1}$$

Here, $M^f(H)$ is the contribution of ferromagnetic (f) nanoparticles (multiple domains and $M^{sp}(H)$ is the contribution from the superparamagnetic (sp) nanoparticles (single domain). Further, the effect of size dispersion is presented in a real system. The magnetization of superparamagnetic nanoparticles can be represented by the expression [31]

$$M^{sp}(H) = M^{sp}(\infty)\sum_j f(m_j) L\left[\frac{m_j H}{K_B T}\right] \tag{2}$$

For particle with sphere shape, the distribution of particle size $f(D)$ is given by the expression [32]

$$f(D) = \frac{1}{\sqrt{2\pi}\sigma D}\exp\left(-\frac{In(D/\bar{D}^2}{2\sigma^2}\right) \tag{3}$$

where, σ is the standard deviation and $\bar{D}$ is the average particle size. $f(m_j)$ can be calculated from D. Figure 3 shows the curve of the $LaFeO_3$ nanostructures with fitting results in Langevin function [32]. The results indicate that the magnetization of $LaFeO_3$ nanopetals is higher than all other $LaFeO_3$ morphologies. The magnetic moment of the antiferromagnetic $LaFeO_3$ nanoparticles originate from the spin uncompensation at the surface and due to the canting of Fe–Fe antiferromagnetic order. As the particle size decreases, an increasing fraction of atoms lie at or near the surface and then the spin uncompensation increases. Hence, the moment of an antiferromagnetic particle is expected to increase significantly with decreasing particle size. The magnetic properties are intimately tied to the Fe–O–Fe bonding of the FeO_6 octahedra [33], which can be attributed to the larger size of $LaFeO_3$ nanopetals than the other nanostructures. The results demonstrate that the $LaFeO_3$ nanostructures exhibit weak ferromagnetism which corresponds with its bulk form [31]. So, we deduce that the magnetic behaviour of the $LaFeO_3$ nanostructures originate from their shape and finite size.

Further, the coercivity value varies from a particular morphology to another significantly. The coercivity value speculated from the hysteresis loop for the nanopetals was 226 Oe followed by the dendrites (205 Oe), nanorods (198 Oe) and nanospheres (59 Oe).

The bigger particles give a higher coercivity Hc. This is in good agreement with the law (Hc–D^6) of the nanomagnetic particles [34]. Generally, the presence of surfactant is claimed to be one of the factors affecting the magnetic properties of the sample. The influence of the surfactant can be of two types. The presence of surfactant can lead to the formation of a non-magnetic dead layer on the surface of the sample, which decrease the overall magnetization. In certain cases, the surfactant acts as a structure directing agent which is responsible for the formation of different morphologies and finally get removed completely during the reaction at elevated temperature and subsequent washing of the samples. In such cases, the surfactant do not directly influence the magnetic properties, rather on the shape and size of the nanostructures.

The shape anisotropy observed might be the sole factor responsible for the variation of magnetic parameters. This shape dependent magnetic behaviour is more pronounced when the particle deviates from the usual spherical shape to anisotropic morphologies. It has been well established that the coercivity increases with increase in shape anisotropy. In the present case, $LaFeO_3$ nanopetals are relatively more anisotropy than the dendrites, nanorods and nanospheres. No obvious loop shift was found in the hysteresis loop of the nanostructures other than nanopetals. Loop shift originates from the interface effect, i.e., the exchange coupling between the spins of the disordered surface and the antiferromagnetic core [35, 36]. It was found to be more dependent on the particle size and shape. The size of

$LaFeO_3$ nanopetals is relatively large and hence the loop shift can be observed. On the other hand, since the $LaFeO_3$ nanospheres are composed of very small grains, loop shift was not observed. From the above results we confirm that the morphologies play a major role in controlling the value of coercivity. In addition to the shape anisotropy, the presence of PSD grain leads to the increase in the coercivity. The reduction in particle size by the surfactant assisted reaction leads to a transformation from PSD to SPM range, which contribute to the decreased coercivity. Thus, the relatively high coercivity of nanopetals compared to the dendrites and nanorods might be due to the combined influence of shape anisotropy and smaller particles in the PSD range which are helpful to the surface spins to form net moment. While $LaFeO_3$ nanospheres is not affected by the shape anisotropy, the surface effect (surface anisotropy) can be observed which exhibits SPM effect. The values of H_c, M_r, and M_r/M_s are shown in the inset of Fig. 3a–d. The weak ferromagnetic behaviour is due to the small particle size and in turn the lower M_r/M_s. Thus, the ratio M_r/M_s could be used as a functional parameter for evaluating the homogeneity on the dimension of nanoparticles. Finally, we found that all $LaFeO_3$ nanostructures behave as a weak ferromagnetic material at room temperature.

3.4 Electrical impedance analysis of different $LaFeO_3$ nanostructures

The electrical impedance and dielectric behavior of the nanostructured perovskite ceramics depend on the chemical composition, shape and size effect. When perovskite materials are sintered under special conditions, the valance state of ions change, and the individual cations thus formed in the sample lead to high conductivity [37].

When such a material is cooled in an oxygen atmosphere, it transforms to a material with high resistivity over the constituent grains. Studies on the effect of temperature, shape, size and frequency on the dielectric behavior and electrical impedance offer valuable information about the conduction phenomenon based on the localized electric charge in the nanostructured $LaFeO_3$ ceramics. The frequency dependence of the electrical impedance was determined in the frequency range between 20 and 10^6 Hz during the temperature plateau for nanostructured $LaFeO_3$ nanopetals, dendrites, nanorods and nanospheres. In Fig. 4a, the complex Cole–Cole (or Nyquist) plot [−Im(Z) vs. Re(Z)] consists of a well resolved semicircle whose center is located below the real axes, i.e., a non Debye behavior, and a spike at low frequencies for a selected ceramic of $LaFeO_3$ nanopetals at room temperature. The spike is an evidence of the electrode polarization effect during our measurements [38]. Besides, these behaviors were found for all $LaFeO_3$ ceramics with different morphologies. In order to describe the complex impedance of materials, we employed a phenomenological model based on two serial (R_1//CPE_1) and (R_2//CPE_2) elements associated with two distinct contributions to the impedance response: one at low frequency and one at high frequency. The total electrical impedance is given by:

$$Z = \left[\frac{1}{R_1} + \frac{1}{Z_{CPE,1}}\right]^{-1} + \left[\frac{1}{R_2} + \frac{1}{Z_{CPE,2}}\right]^{-1} \quad (4)$$

In both cases, CPE (constant phase element) denotes the pseudo capacitance defined by Jonscher [39]. The impedance of CPE is expressed as follows [40].

$$Z_{CPE} = \frac{1}{Q(j\omega)^{\alpha}} \quad (5)$$

where Q is a CPE constant in $F \cdot s^{\alpha-1}$, $\omega = 2\pi f$ is the angular frequency (f being the frequency in Hz), α is the dimensionless CPE parameter ranging from 0 up to 1, and $j = \sqrt{-1}$ is the imaginary unit. The equivalent circuit based on the impedance data for the nanopetals sample is shown in Fig. 4a inset. Probably, the occurrence of one semicircle indicates that the grain and grain boundary are overlapped owing to the similar relaxation frequency of both contributions or the grain boundary conduction is almost negligible. Therefore, the parameter R_1 denotes the total resistance of the dc-resistances R_b and R_{gb} associated to the grain and grain boundary. The parameters of Eq. (4) were obtained for three different temperatures (300, 310, and 320 K) for all the nanostructures by analyzing the data using the non-linear least squares (NLLS) fitting procedure, as illustrated in Fig. 4b for the ceramic $LaFeO_3$ nanopetals at room temperature. Then, the total conductivity (σ_{DC}) is the sum of the two conductivities of both grain and grain boundary ($\sigma_{DC} = \sigma_g + \sigma_{gb}$). From Fig. 4c, we note that the total resistance of the $LaFeO_3$ nanopetals ceramic decreases with the increase in temperature suggesting that the total conductivity is a thermally activated quantity. These behaviors were also found for all ceramics with different morphologies.

From Fig. 4d, the activation energies for the total conductivity are found to be in the range 0.110, 0.120, 0.137 and 0.142 eV for $LaFeO_3$ nanopetals, dendrites, nanorods and nanospheres. The values of activation energies are characteristic of the electron hopping between Fe^{2+} and Fe^{3+} ions in B sites (electronic conductivity). Therefore, the conduction due to anion vacancies may be responsible for the conductivity behavior with higher activation energy ($\sim$0.142 eV) in the high temperature region for nanospheres with grain size (50 nm). Probably, the different activation energy values may be explained based on the variation of the zero point energy induced by the powder morphology. According to Rodrigues *et al.* [41], a system with lower vibrational frequencies will have a lower zero-

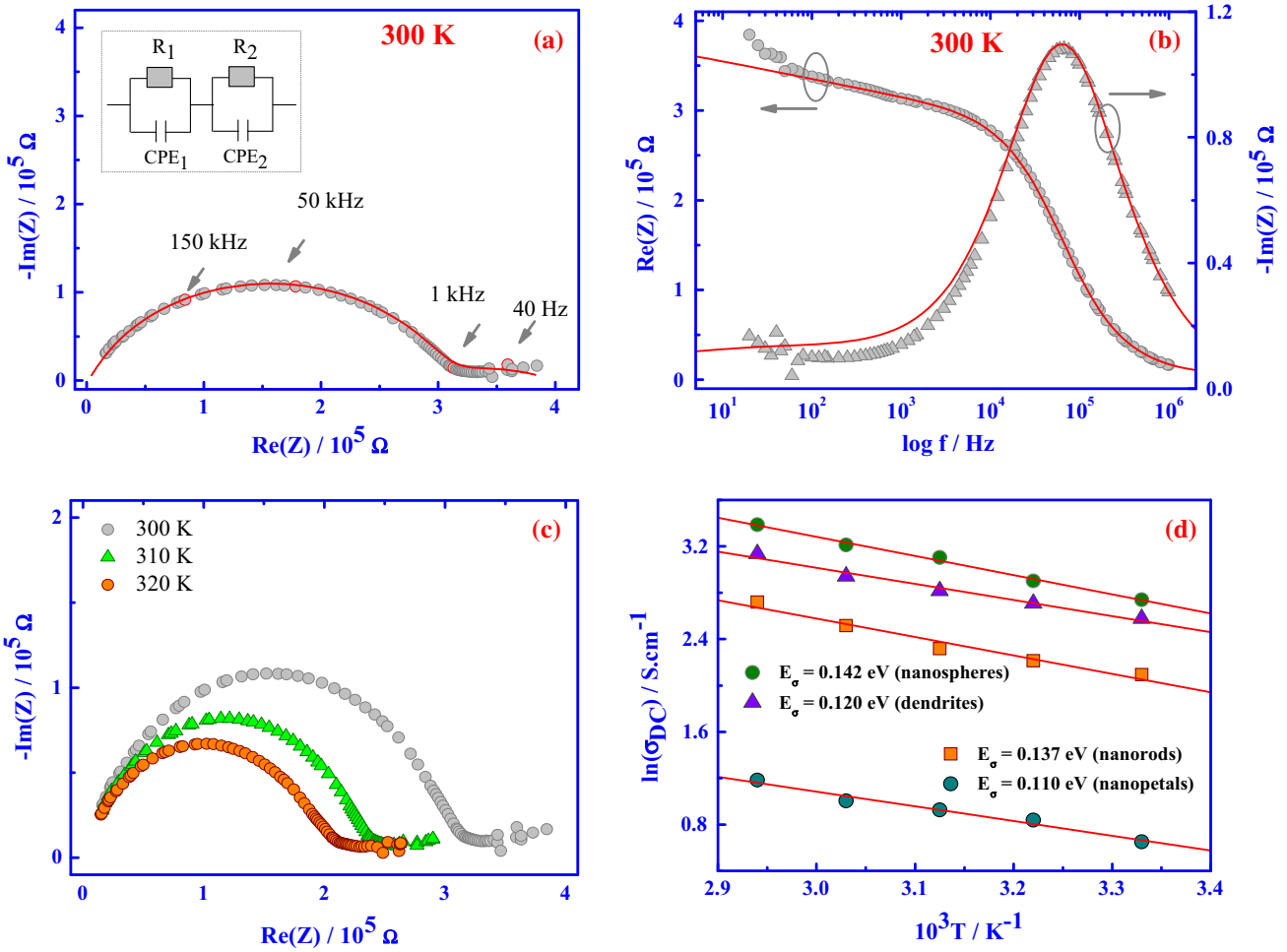

Fig. 4 Impedance spectra for $LaFeO_3$ nanopetals **a** room temperature, **b** real part Re(Z*) and the opposite of the imaginary part—Im(Z*) as a function of frequency at RT, **c** impedance spectra at different temperatures and **d** Arrhenius plot of the conductivity for different $LaFeO_3$ nanostructures

point energy and higher activation energy. In addition, a variation in the vibrational frequency is induced by the size effect in nanomaterial [42]. Therefore one can concludethat the size and morphology of the $LaFeO_3$ nanoparticles changed the vibrational frequencies associated with iron and oxygen motions in the octahedral cage, resulting in the variation of activation energy values during the electronic conductivity process. The value of activation energy exhibited by nanospheres is characteristic to the diffusion of oxygen vacancies. For the $LaFeO_3$ nanostructures (nanopetals, dendrites and nanorods) with grain size in the range ~60–90 nm (as discussed in the XRD and TEM analysis), the number of oxygen vacancies is expected to be negligible, so that conduction is mostly due to the charge carriers [43]. The conduction mechanism of $LaFeO_3$ nanostructures can be explained on the basis of hopping of the charge carriers between Fe^{2+} and Fe^{3+} on the octahedral sites. The compositional dependence on ac conductivity is also depicted. It can be evidenced that the magnitude of conductivity increases with decrease in grain size. The maximum conductivity was obtained for nanospheres, which could be attributed to the increased active carrier concentration with decreased grain size.

3.5 Dielectric behaviour of different $LaFeO_3$ nanostructures

3.5.1 Frequency dependence

The effect of frequency (ω) dependence on the dielectric constant ε′ and dielectric loss factor tan δ (at 300 K) for samples with various morphology of $LaFeO_3$ nanostructures possessing different size are illustrated in Fig. 5a, b respectively.

From Fig. 5a, we observe that all the samples reveal frequency-dependent phenomena. This is a normal behaviour observed in most of the weak ferromagnetic materials, which could be attributed to interfacial polarization as described by

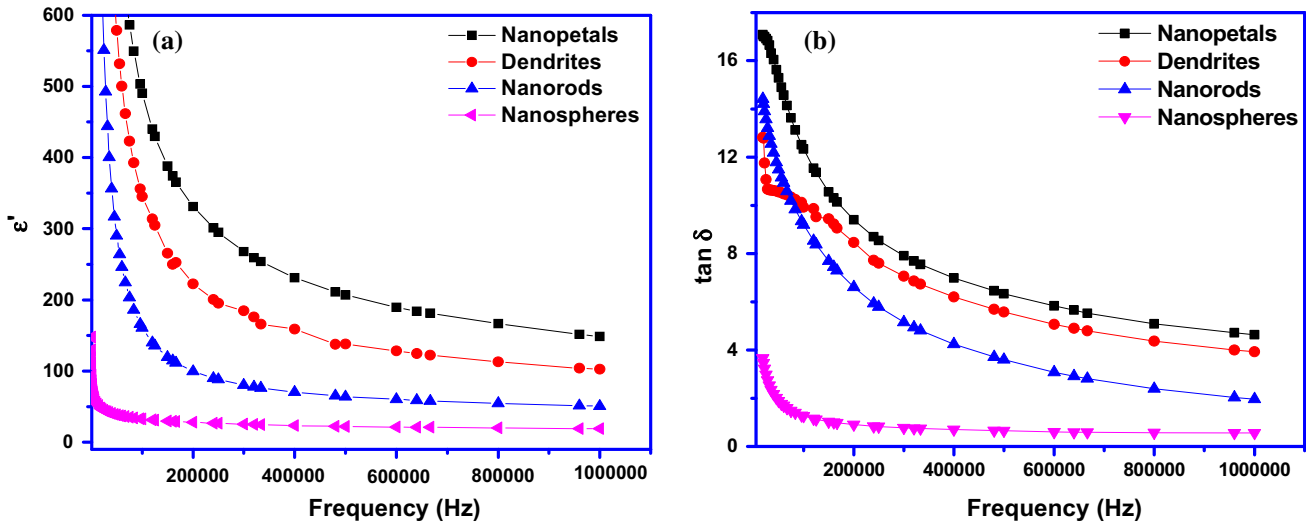

Fig. 5 **a** Real part ε′ of the dielectric constant at 300 K and **b** dielectric loss factor tan δ at 300 K as a function of frequency for the different $LaFeO_3$ nanostructures

Wagner [44]. It is observed that the dielectric constant decreases with increasing frequency, and becomes almost steady at higher frequency. The variation in dielectric constant with frequency is explained on the basis of space charge polarization [45]. The space charge polarization rises due to the inhomogeneous dielectric structure of the material. The existence of Fe^{3+} ions and the minority Fe^{2+} ions have rendered the $LaFeO_3$ dipolar. Rotational displacement of the dipoles results in orientation polarization. In the case of $LaFeO_3$, the rotation of $Fe^{2+} \leftrightarrow Fe^{3+}$ dipoles may be visualized as the exchange of electrons between the ions, so that the dipoles align themselves with the alternating field [46]. The existence of inertia to the charge movement would cause a relaxation to the polarization. Among all the compounds, the dielectric constant value observed at all measured frequencies for the different $LaFeO_3$ nanostructures was low because all the samples show p-type conduction due to the hole exchange between La^{3+} and La^{4+} [47].

The dielectric loss tan δ shown in Fig. 5b exhibits an anomalous behaviour with frequency for the $LaFeO_3$ nanostructures and decreases with increasing frequency. In the normal behaviour, the polarization (or dielectric constant) will monotonically decrease with frequency as in the case of $LaFeO_3$ nanopetals, dendrites, nanorods and nanospheres. This happens as the electronic exchange between $Fe^{2+} \leftrightarrow Fe^{3+}$ cannot follow the alternating field beyond a certain frequency. In $LaFeO_3$ nanostructures, the presence of La^{3+} and La^{4+} ions gives rise to p-type carriers. The local displacements of p-type carriers in the direction of the external electric field also contribute to the net polarization. However, the contribution of p-type carriers should be smaller than the electronic exchange between $Fe^{2+} \leftrightarrow Fe^{3+}$. Since the mobility of the p-type carriers is smaller than the n-type carriers, the contribution to polarization from the former will decrease more rapidly even at lower frequencies than from the latter. The shift in the position of the maximum towards lower frequencies when the grain size is reduced can be explained by proposing a decrease in the number of p-type carriers in the B sites as reported elsewhere [48]. The real part of the dielectric constant decreases with increase in frequency and also the dielectric loss is lower for smaller grain size as the resistivity increases with grain size reduction. The value of dielectric constant ε′ and the dielectric loss δ for the $LaFeO_3$ nanopetals, dendrites, and nanorods were found to be one order of magnitude higher than the $LaFeO_3$ nanospheres. Similarly, all the $LaFeO_3$ nanostructures were found to be two orders of magnitude better than other reported perovskite oxide materials [47].

3.5.2 *Temperature dependence*

The anomalous temperature dependence of dielectric constant ε′ for different $LaFeO_3$ nanostructures represented in Fig. 6a could be explained on the basis of its frequency dependence. The contribution of the carrier towards polarization depends on the temperature, which influence the electronic exchange of $Fe^{2+} \leftrightarrow Fe^{3+}$ more than the displacement of p-type carriers. The value of dielectric constant ε′ changes from one morphology to another. The different morphologies of $LaFeO_3$ nanostructures contain enormous number of interfaces, and the large number of defects present in these interfaces can cause a change in the positive or negative space charge distribution. When an electric field is applied, these space charges move and are trapped by the defects resulting in the formation of dipole moments. This is called space charge polarization [49].

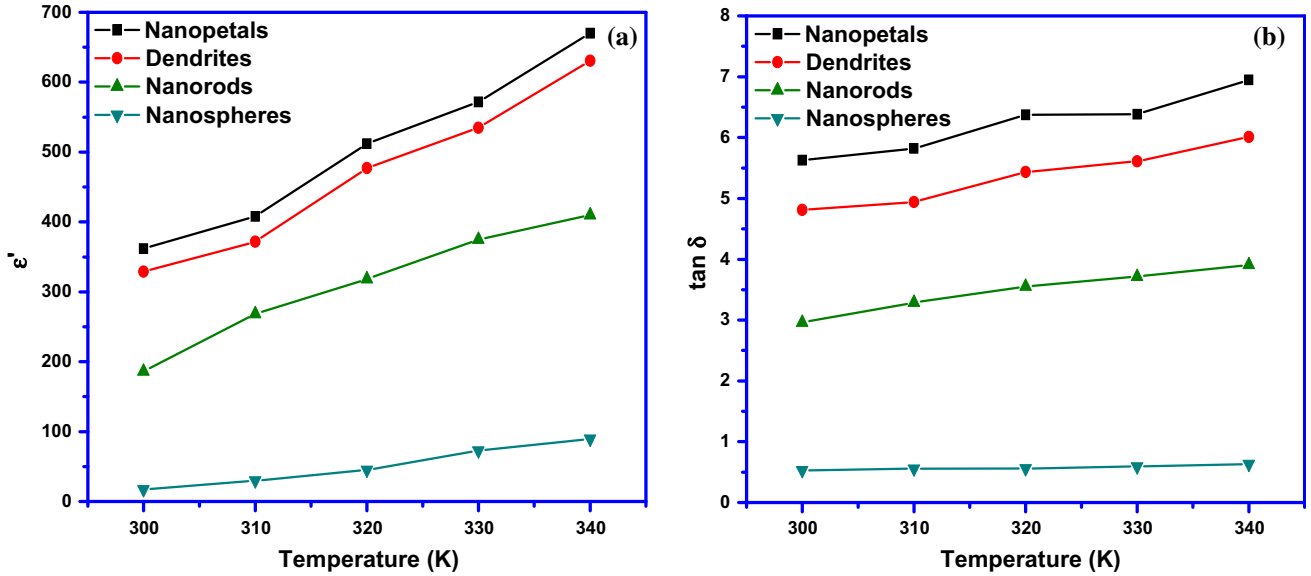

Fig. 6 **a** Real part ε′ of the dielectric constant at 1000 Hz and **b** dielectric loss factor tan δ at 1000 Hz as a function of temperature for the different $LaFeO_3$ nanostructures

The interfaces in $LaFeO_3$ nanostructure material posses some oxygen ion vacancies which are equivalent to the positive charges giving dipole moments. When exposed to an electric field these dipoles will rotate, giving a resultant dipole moment in the direction of the applied field. In the present study, all $LaFeO_3$ morphologies at low temperature are mainly due to the space charge polarization and rotation direction polarization [50, 51]. As the temperature increases, more and more dipoles will be oriented in the direction of the applied field resulting in the increase of dipole moment value [52]. The variation of dielectric loss (tan δ) for different morphology and size are due to the shape and size effect as observed in Fig. 6b. The volume percentage of interface boundaries and therefore the amount of defects that causes the various types of polarization increase as the particle size is reduced. The hopping or jumping probability per unit time increases with increase in temperature. Correspondingly, the loss tangent decreases with grain size reduction [53]. Further there exists strong correlation between the conduction mechanism and the dielectric behaviour. The conduction mechanism is due to the hopping of electrons; as such when the hopping frequency is nearly equal to the frequency of the externally applied electric field, a maximum of loss tangent may be observed.

4 Conclusions

In summary, the magnetic and electrical properties are highly dependent on the size and shape of the $LaFeO_3$ nanostructures. Structural analysis confirmed the formation of orthorhombic single phase and the TEM results reveal the well-shaped different morphologies with smaller size. The room temperature weak ferromagnetism behaviour was confirmed from the VSM analysis for the prepared different $LaFeO_3$ nanostructures. The values of activation energy obtained are characteristic of the hopping charge carriers. The activation energy slightly increases with the grain size reduction due to the blocking nature of the associated grain boundary. Dielectric properties for $LaFeO_3$ nanopetals, dendrites, and nanorods are found to be one order of magnitude higher than the $LaFeO_3$ nanospheres and all the $LaFeO_3$ nanostructures were found to be two orders of magnitude better than other reported perovskite oxide materials. Finally, the excellent combination of magnetic and electric properties of $LaFeO_3$ nanostructure materials was found to be suitable for use in high-frequency applications.

Acknowledgments One of the author S. T gratefully acknowledges Jawaharlal Nehru Memorial Fund for Doctoral studies (Ref: SU-A/270/2011-2012/388 dated 09-12-2010) and also Brazilian research financing institutions: CAPES, FAPESP/CEPID 2013/19049-0, INCTMN/CNPq and FAPESP for financial aid.

References

1. K. Mukhopadhyay, A.S. Mahapatra, P.K. Chakrabarti, Multiferroic behavior, enhanced magnetization and exchange bias effect of Zn substituted nanocrystalline $LaFeO_3(La_{(1-x)}Zn_xFeO_3$, $x = 0.10$, and 0.30). J. Magn. Magn. Mater. **329**, 133–141 (2013)
2. J. Yoo, S. Kim, H. Choi, Y. Rhim, J. Lim, S. Lee, A.J. Jacobson, Size effect on magnetic and dielectric properties in nanocrystalline $LaFeO_3$. J. Electroceram. **26**, 56–62 (2011)

3. E.V. Tsipis, M.V. Patrakeev, V.V. Kharton, A.A. Yaremchenko, G.C. Mather, A.L. Shaula, I.A. Leonidov, V.L. Kozhevnikov, J.R. Frade, Transport properties and thermal expansion of Ti-substituted $La_{1-x}Sr_xFeO_{3-\delta}$ (x = 0.5–0.7). Solid State Sci. **7**, 355–365 (2005)
4. A.H. Wu, H. Shen, J. Xu, L.W. Jiang, L.Q. Luo, S.J. Yuan, S.X. Cao, H.J. Zhang, Preparation and magnetic properties of $RFeO_3$ nanocrystalline powders. J. Sol-Gel Sci. Technol. **59**, 158–163 (2011)
5. P. Pramanik, R.N. Das, Structure property relations of chemically synthesized nanocrystalline PZT powders. Mater. Sci. Eng. A **304–306**, 775–779 (2001)
6. K. Girija, S. Thirumalairajan, D. Mangalaraj, Morphology controllable synthesis of parallely arranged single-crystalline β-Ga_2O_3 nanorods for photocatalytic and antimicrobial activities. Chem. Eng. J. **236**, 181–190 (2014)
7. R.J. Cava, B. Batlogg, J.J. Krajewski, R. Farrow, L.W. Rupp Jr, A.E. White, K. Short, W.F. Peck, T. Kometani, Superconductivity near 30 K without copper: the $Ba_{0.6}K_{0.4}BiO_3$ perovskite. Nature **332**, 814–816 (1988)
8. Y. Tokura, Y. Tomioka, Colossal magnetoresistive manganites. J. Magn. Magn. Mater. **200**, 1–23 (1999)
9. S.D. Shenoy, P.A. Joy, M.R. Anantharaman, Effect of mechanical milling on the structural, magnetic and dielectric properties of coprecipitated ultrafine zinc ferrite. J. Magn. Magn. Mater. **269**, 217–226 (2004)
10. S. Huang, K. Ruan, Z. Lv, P. Wei, H. Wu, M. Li, J. Zhang, Y. Chai, H. Yang, L. Cao, X. Li, Magnetic and transport properties in layered $Nd_{1-x}Sr_{1+x}CoO_4$. Phys. Rev. B Condens. Matter Mater. Phys **73**, 094431 (2006)
11. Y. Shimada, S. Miyasaka, R. Kumai, Y. Tokura, Semiconducting ferromagnetic states in $La_{1-x}Sr_{1+x}CoO_4$. Phys. Rev. B Condens. Matter Mater. Phys. **73**, 134424 (2006)
12. P. Porta, S. De Rossi, M. Faticanti, G. Minelli, I. Pettiti, L. Lisi, M. Turco, Perovskite-type oxides: I. structural, magnetic, and morphological properties of $LaMn_{1-x}Cu_xO_3$ and $LaCo_{1-x}Cu_xO_3$ solid solutions with large surface area. J. Solid State Chem. **146**, 291–304 (1999)
13. D. Cordischi, M. Faticanti, G. Minelli, M. Occhiuzzi, P. Porta, $LaAl_{1x}Cr_xO_3$ perovskite-type solid solutions: structural, electronic, magnetic properties and catalytic activity towards CO oxidation. Phys. Chem. Chem. Phys. **4**, 3085–3090 (2002)
14. P. Singh, D. Kumar, O. Parkash, Dielectric behaviour of the system $BaSn_{1-x}Nb_xO_3$ ($x \leq 0.10$). J. Appl. Phys. **97**, 074103 (2005)
15. Q. Liu, J. Dai, Z. Liu, X. Zhang, G. Zhu, G. Ding, Electrical and optical properties of Sb-doped $BaSnO_3$ epitaxial films grown by pulsed laser deposition. J. Phys. D Appl. Phys. **43**, 455401 (2010)
16. X. Luo, Y.S. Oh, A. Sirenko, P. Gao, T.A. Tyson, K. Char, S.W. Cheong, High carrier mobility in transparent $Ba_{1-x}La_xSnO_3$ crystals with a wide band gap. Appl. Phys. Lett. **100**, 172112 (2012)
17. W.B. Li, J.X. Wang, H. Gong, Catalytic combustion of VOCs on non-noble metal catalysts. Catal. Today **148**, 81–87 (2009)
18. J. Lojevska, A. Kolodziej, J. Zak, J. Stoch, Pd/Pt promoted Co_3O_4 catalysts for VOCs combustion: preparation of active catalyst on metallic carrier. Catal. Today **105**, 655–661 (2005)
19. Y. Masuda, K. Kato, Liquid-phase patterning and microstructure of anatase TiO_2 films on SnO_2: F substrates using super hydrophilic surface. Chem. Mater. **20**, 1057–1063 (2008)
20. J.H. Su, L.Q. Jing, K. Shi, H.G. Fu, Synthesis of large surface area $LaFeO_3$ nanoparticles by SBA16 template method as high active visible photocatalysts. J. Nanopart. Res. **12**, 967–974 (2010)
21. R.H. Kodama, A.E. Berkowitz, S. Foner, Surface spin disorder in $NiFe_2O_4$ nanoparticles. Phys. Rev. Lett. **77**, 394 (1996)
22. M.L. Billas, A. Chatelain, W.A. de Heer, Magnetism from the atom to the bulk in iron, cobalt, and nickel clusters. Science **265**, 1682 (1994)
23. J. Shi, S. Gider, K. Babcock, D.D. Awschalom, Magnetic clusters in molecular beams, metals, and semiconductors. Science **271**, 937 (1996)
24. S. Thirumalairajan, K. Girija, I. Ganesh, D. Mangalaraj, C. Viswanathan, A. Balamurugan, N. Ponpandian, Controlled synthesis of perovskite $LaFeO_3$ microsphere composed of nanoparticles via self-assembly process and their associated photocatalytic activity. Chem. Eng. J. **209**, 420–428 (2012)
25. S. Thirumalairajan, K. Girija, I. Ganesh, D. Mangalaraj, C. Viswanathan, N. Ponpandian, Novel synthesis of $LaFeO_3$ nanostructure dendrites: a systematic investigation of growth mechanism, properties, and biosensing for highly selective determination of neurotransmitter compounds. Cryst. Growth Des. **13**, 291–302 (2013)
26. S. Thirumalairajan, K. Girija, N.Y. Hebalkar, D. Mangalaraj, N. Ponpandian, Shape evolution of perovskite $LaFeO_3$ nanostructures: a systematic investigation of growth mechanism, properties and morphology dependent photocatalytic activities. RSC Adv. **3**, 7549–7561 (2013)
27. S. Thirumalairajan, K. Girija, V.R. Mastelaro, N. Ponpandian, Photocatalytic degradation of organic dyes under visible light irradiation by floral-like $LaFeO_3$ nanostructures comprised of nanosheet petals. New J. Chem. **38**, 5480–5490 (2014)
28. M.C. Carotta, M.A. Butturi, Y. Sadaoka, Microstructural evolution of nanosized $LaFeO_3$ Powders from the thermal decomposition of a cyano-complex for thick film gas sensors. Sens. Actuators B **44**, 590–594 (1997)
29. M. Kumar, B. Ravikumar, T.C. Alex, Synthesis of pure and Sr-doped $LaGaO_3$, $LaFeO_3$ and $LaCoO_3$ and SrMg-doped $LaGaO_3$ for ITSOFC application using different wet chemical routes. Mater. Chem. Phys. **113**, 803–815 (2009)
30. F. Munakata, H. Takahashi, Y. Akimune, Y. Shichi, M. Tanimura, Y. Inoue, R. Itti, Y. Koyama, Phys. Rev. B Condens. Matter Mater. Phys. **56**, 979 (1997)
31. F.C. Fonseca, A.S. Ferlauto, F. Alvarez, G.F. Goya, R.F. Jardim, Morphological and magnetic properties of carbon–nickel nanocomposite thin films. J. Appl. Phys. **97**, 044313 (2005)
32. S.J. Lee, J.R. Jeong, S.C. Shin, J.C. Kim, J.D. Kim, Synthesis and characterization of superparamagnetic maghemite nanoparticles prepared by co-precipitation technique. J. Magn. Magn. Mater. **282**, 147–150 (2004)
33. N. Gayathri, A.K. Raychaudhuri, S.K. Tiwary, Electrical transport, magnetism, and magnetoresistance in ferromagnetic oxides with mixed exchange interactions: a study of the $La_{0.7}Ca_{0.3}$-$Mn_{1-x}Co_xO_3$ system. Phys. Rev. B Condens. Matter Mater. Phys. **56**, 1345–1353 (1997)
34. D. Xue, G. Chai, X. Li, X. Fan, Effects of grain size distribution on coercivity and permeability of ferromagnets. J. Magn. Magn. Mater. **320**, 1541–1543 (2008)
35. R. Mazumder, P.S. Devi, D. Bhattacharya, P. Choudhury, A. Sen, M. Raja, Ferromagnetism in nanoscale $BiFeO_3$. Appl. Phys. Lett. **91**, 062510 (2007)
36. S. Vijayanand, H.S. Potdar, P.A. Joy, Origin of high room temperature ferromagnetic moment of nanocrystalline multiferroic $BiFeO_3$. Appl. Phys. Lett. **94**, 182507 (2009)
37. E. Barsoukov, J.R. Macdonald, *Impedance Spectroscopy: Theory, Experiment, and Applications*, 2nd edn. (Wiley, New York, 2005)
38. M. Malki, C.M. Hoo, M.L. Mecartney, H. Schneider, Electrical conductivity of mullite ceramics. J. Am. Ceram. Soc. **97**, 1923–1930 (2014)
39. A.K. Jonscher, The universal dielectric response and its physical significance. IEEE Trans. Electr. Insul. **27**, 407 (1992)

40. J.B. Jorcin, M.E. Orazem, N. Pébère, B. Tribollet, CPE analysis by local electrochemical impedance spectroscopy. Electrochim. Acta **51**, 1473–1479 (2006)
41. J.E.F.S. Rodrigues, C.W.D.A. Paschoal, E.N. Silva, K.A. Mince, M.W. Lufaso, Relaxations in Ba_2BiTaO_6 ceramics investigated by impedance and electric modulus spectroscopies. Mater. Res. Bull. **47**, 878–882 (2012)
42. G. Gouadec, P. Colomban, Raman Spectroscopy of nanomaterials: how spectra relate to disorder, particle size and mechanical properties. Prog. Cryst. Growth Charact. Mater. **53**, 1 (2007)
43. I. Kosacki, V. Petrovsky, H.U. Anderson, P. Colomban, Raman spectroscopy of nanocrystalline ceria and zirconia thin films. J. Am. Ceram. Soc. **85**, 2646–2650 (2004)
44. M. Tian, S.L. Yuan, X.L. Wang, X.F. Zheng, S.Y. Yin, C.H. Wang, L. Liu, Bifunctional properties of hydrothermal synthesized $BaMF_4$ (M = Co, Ni and Zn). J. Appl. Phys. **106**, 103912 (2009)
45. C.W. Wu, Y.H. Nan, Y. Lin, Deng, giant dielectric permittivity observed in Li and Ti doped NiO. Phys. Rev. Lett. **89**, 217601 (2002)
46. M. Idrees, M. Nadeem, M. Mehmood, M. Atif, K.H. Chae, M.M. Hassan, Impedance spectroscopic investigation of delocalization effects of disorder induced by Ni doping in $LaFeO_3$. Acta Mater. **44**, 105401 (2011)
47. M. Idrees, M. Nadeem, M. Atif, M. Siddique, M. Mehmood, M.M. Hassan, Origin of colossal dielectric response in $LaFeO_3$. Acta Mater. **59**, 1338–1345 (2011)
48. S. Javaid, M.J. Akhtar, Pressure-induced magnetic, structural, and electronic phase transitions in LaFeO3: a density functional theory (generalized gradient approximation) + U study. J. Appl. Phys. **116**, 023704 (2014)
49. Z. Zanolli, J.C. Wojdeł, J. Íñiguez, P. Ghosez, Electric control of the magnetization in $BiFeO_3/LaFeO_3$ superlattices. Phys. Rev. B Condens. Matter Mater. Phys. **88**, 060102 (2013)
50. N.T. Padal, S.A. Pawar, Y.D. Kolekar, S.V. Kulkarni, P.B. Joshi, Structural, dielectric and electron transport properties of $LaFeO_3$ substituted (PbBa) TiO_3 ferroelectrics. Ferroelectrics **323**, 123–129 (2005)
51. I. Wærnhus, P.E. Vullum, R. Holmestad, T. Grande, K. Wiik, Electronic properties of polycrystalline $LaFeO_3$. Part I: experimental results and the qualitative role of Schottky defects. Solid State Ion. **176**, 2783–2790 (2005)
52. P. Kanhere, J. Nisar, Y. Tang, B. Pathak, R. Ahuja, J. Zheng, Z. Chen, Electronic structure, optical properties, and photocatalytic activities of $LaFeO_3$–$NaTaO_3$ solid solution. J. Phys. Chem. C **116**, 22767–22773 (2012)
53. G.R. Hearne, M.P. Pasternak, R.D. Taylor, P. Lacorre, Electronic structure and magnetic properties of $LaFeO_3$ at high pressure. Phys. Rev. B Condens. Matter Mater. Phys. **51**, 11495–11500 (1995)